Advances in Water Resources 122 (2018) 131–138

Contents lists available at ScienceDirect

Advances in Water Resources

journal homepage: www.elsevier.com/locate/advwatres

Impact of uncertainty in soil texture parameters on estimation of soil moisture through radio waves transmission

E. Di Fusco[a], I. Lauriola[a], R. Verdone[b], V. Di Federico[a], V. Ciriello[a,*]

[a] Dipartimento di Ingegneria Civile, Chimica, Ambientale e dei Materiali (DICAM), Università di Bologna, Bologna, Italy
[b] Department of Electrical, Electronic and Information Engineering "Guglielmo Marconi" (DEI), Università di Bologna, Bologna, Italy

ARTICLE INFO

Keywords:
Global sensitivity analysis
Soil moisture
Wireless underground communication networks
Soil texture
Subsurface hydrology

ABSTRACT

Soil moisture is a key parameter which governs the soil water balance and affects hydrologic processes such as water infiltration and evapotranspiration. These processes are critical in several fields related to water resources including precision agriculture and drought management. As such, increasing attention is paid to field estimation of soil moisture. Indirect methods are generally preferred as they are non-destructive and measures can be detected almost continuously in time. Among indirect methods, here we focus on wireless underground communication networks (WUCNs) which is a promising technique based on the transmission of radio waves to a buried collector. From measurements of the electromagnetic loss, and based on either single path or two-path models, information on soil moisture can be retrieved. In this context, we perform global sensitivity analysis (GSA) to investigate how parametric uncertainty associated with soil texture, plagues soil moisture predictions. This is critical to identify which texture parameters require accurate estimation to narrow the uncertainty associated with predictions in practical applications. In particular, we study the influence of porosity and of sand and clay contents and found significantly different results for diverse soil types, thus suggesting the importance of a preliminary GSA to guide the design of measurement campaigns on field.

1. Introduction

1.1. Wireless underground communication networks

Soil moisture is a key quantity in the field of drought management and to close the soil water balance in hydrologic modeling. It also plays a critical role in precision agriculture for enabling flexible and smart irrigation strategies (e.g., Ahmad et al., 2018; Huang et al., 2017; Martnez-Fernndez et al., 2015; Moghadas et al., 2017; Narasimhan and Srinivasan, 2005; Sheffield and Wood, 2008).

Soil moisture can be measured directly through the gravimetric method, which is however a destructive time-consuming approach, difficult to use in practical applications. Due to these limitations, several indirect methods have been developed to provide a measure of another quantity that can be related to soil moisture through physically based and empirical equations. A widely used technology, focused on dielectric measurements, is time domain reflectometry (TDR), which has shown to be more accurate and economical if compared to frequency domain reflectometry (FDR). However, both these technologies provide local scale (single point) measures. In order to move towards field scale measures one may resort to geophysical methods such as ground penetrating radar (GPR), that is however an expensive technology, or electrical resistivity measurements, with the disadvantage that data acquisition is periodic or requires regular field surveys (for more details on indirect methods see e.g. Bittelli, 2011; Dobriyal et al., 2012, and references therein).

In this context, a recent and promising monitoring technique consists (in the basic configuration) of two radio transceivers (hereinafter denoted as devices), buried underground, that can exchange signals and make possible to provide indirect estimates of soil moisture without the need for an ad hoc device, based on the idea that radio waves propagate through the soil with a loss rate which depends on the volumetric water content (e.g., Akyildiz and Stuntebeck, 2006; Akyildiz et al., 2009; Dong et al., 2013; Vuran and Silva, 2009, and references therein). In addition, this approach provides an average estimate over the transmission volume instead of a single point measure. Soil moisture is measured locally and then transmitted by the receiving node to a surface gateway. The latter will forward data to the Internet through, e.g., a UAV repeater flying above the area. Measuring soil moisture at 30–100 cm depth through devices connected to the Internet may provide critical real time information for several applications.

LoRa is a novel wireless technology for the IoT (Internet of Things) even much more robust to power losses than its predecessors. LoRa operates on ISM bands that are available in the world on a Region and

* Corresponding author.
E-mail address: valentina.ciriello3@unibo.it (V. Ciriello).

https://doi.org/10.1016/j.advwatres.2018.10.007
Received 10 July 2018; Received in revised form 8 October 2018; Accepted 11 October 2018
Available online 11 October 2018

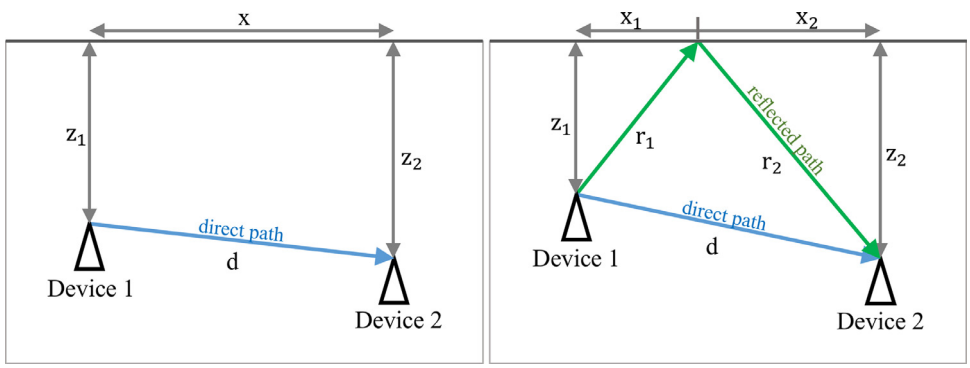

Fig. 1. Possible configurations of WUCNs. In the left panel a single path transmission is depicted, while in the right panel a two-path transmission mechanism is shown due to the reflection produced by the ground surface.

Country-level basis. In ITU Region 1, including Europe, the 863 MHz–870 MHz frequency range can be used by LoRa devices. However, in Countries like Italy, the availability of the band is limited to the range 868–870 MHz. In Region 2 (Americas), the available frequency range is 902 MHz–928 MHz. From the viewpoint of the underground propagation channel, it is expected that no major differences are found between these options. The LoRa technology can provide successful detection of data pockets suffering a power loss of up to 151 dB, when very low data rates are needed. Theoretically, such margin to loss enables to link zones of up to 10 m underground, depending on soil texture and moisture, and the antenna type.

1.2. Mathematical foundation

EM wave propagation in soil can be described with a link budget based on the Friis equation with an additional term accounting for the attenuation induced by the soil with respect to free space propagation (e.g. Li et al., 2007, and references therein). The power of the received signal, P_r $[dB]$, is computed as follows:

$$P_r = P_t + G_r + G_t - L_0 - L_s \tag{1}$$

where P_t $[dB]$ is the transmitted power, G_r $[dB]$ and G_t $[dB]$ are the gains of the receiver and transmitter antennae respectively, L_0 $[dB]$ is the path loss in free space and L_s $[dB]$ the additional path loss due to the soil. These losses are given by:

$$L_0 = 20\log(4\pi d/\lambda), \tag{2}$$

$$L_s = L_\beta + L_\alpha = 20\log\left(\lambda_0/\lambda\right) + e^{2\alpha d}, \tag{3}$$

where d $[m]$ is the distance between devices, L_β $[dB]$ is due to the difference of signal wavelength in soil, $\lambda = 2\pi/\beta$, with respect to the same in free space, $\lambda_0 = c/f$, with β $[rad/m]$ the phase shifting constant and f $[Hz]$ the operating frequency; L_α $[dB]$ is the transmission loss caused by attenuation with attenuation constant α $[1/m]$.

Both α and β depend on the dielectric properties of soil: the permeability, μ $[H/m]$, the conductivity, σ $[S/m]$, and the permittivity, ε $[F/m]$. Let's consider the Helmholtz equations (written in terms of phasor vector equations):

$$\nabla^2 E_s - \gamma^2 E_s = 0 \quad \nabla^2 H_s - \gamma^2 H_s = 0, \tag{4}$$

where E_s is the phasor vector associated with the electric field E $[V/m]$ through the relationship $\partial E/\partial t = i\omega E_s$; the same holds for H_s which is the phasor vector associated with the magnetic field H $[A/m]$ (Balanis, 2012).

In (4), γ is the propagation constant, which is defined as follows

$$\gamma = \sqrt{i\omega\mu(\sigma + i\omega\varepsilon)}, \tag{5}$$

where ω $[rad/s]$ is the angular frequency ($\omega = 2\pi f$). By imposing $\gamma = \alpha + i\beta$, from (5), it is possible to derive the following expressions for α and β as functions of the dielectric soil properties:

$$\alpha, \beta = \omega\sqrt{\frac{\mu\varepsilon}{2}\left[\sqrt{1 + \left(\frac{\sigma}{\omega\varepsilon}\right)^2} \mp 1\right]}. \tag{6}$$

1.3. Impact of soil texture on measurements

Given that the soil consists in a multiphase medium of air, water (both bound and free) and bulk soil, EM wave propagation is generally facilitated in case of low soil density and high porosity combined with low water contents, as the rate of air presence is larger under these conditions. The volumetric moisture content provides a critical contribution to the EM wave attenuation. It includes information about the presence of bound and free water at a time; soil texture analysis, and specifically the quantity of clay in the soil, allows one to distinguish among these two contributions.

Frequency also affects the dielectric constants. The range of frequencies used in practical applications is 0.3–1 GHz, which is associated with reasonable dielectric constants for wireless communication and feasible sizes of the antenna.

From a geometrical point of view, the distance between devices also plays a role as well as the burial depth; in case of low depths underground (generally <0.3–0.5 m) the ground surface produces a reflection/refraction effect which has to be considered. In this case, the received signal consists of two components: a direct path from the transmitter to the receiver and a reflecting path due to the ground surface; a two-path model has to be preferred in this case with respect to the single path conceptualization (see Fig. 1).

The path loss increases with frequency and distance between devices, and is affected by soil moisture and texture in turn. If one uses WUCNs to estimate soil moisture, it is critical to perform preliminary analysis to properly design measurement campaigns under specific field conditions. In particular, it is relevant to identify the influence of soil texture parameters on path loss values, given the uncertainty which typically characterizes the subsurface environment and specifically the vadose zone (e.g., Assouline et al., 2017; Brandhorst et al., 2017; Tartakovsky, 2013).

As such, in this paper we perform a variance-based GSA, through the computation of the Sobol' indices (Sobol', 1993; 2001), to provide an insight in how to reduce predictive uncertainty and properly adopt this monitoring approach in practical applications. To perform GSA, we resort to the equations introduced in Section 1.2 and to a semi-empirical model suggested by Peplinski et al. (1995), which provides expressions for the dielectric properties of soils as function of soil porosity, and clay and sand percentages, in the range 0.3–1.3GHz. The resulting mathematical framework is then reduced by means of an efficient computational algorithm based on the Polynomial Chaos Expansion (PCE)

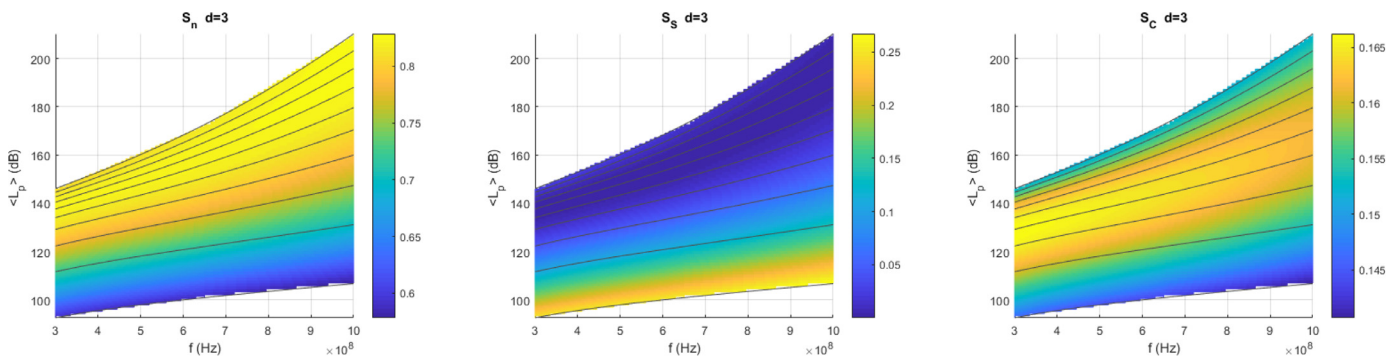

Fig. 2. Single path model: variations of S_n, S_S, S_C in case of clay-loam in the $(\langle L_p \rangle, f)$ plane. Grey lines denote constant values for m_v between 0.05 (the lowest) and 0.5 (the highest), with a constant step of 0.05.

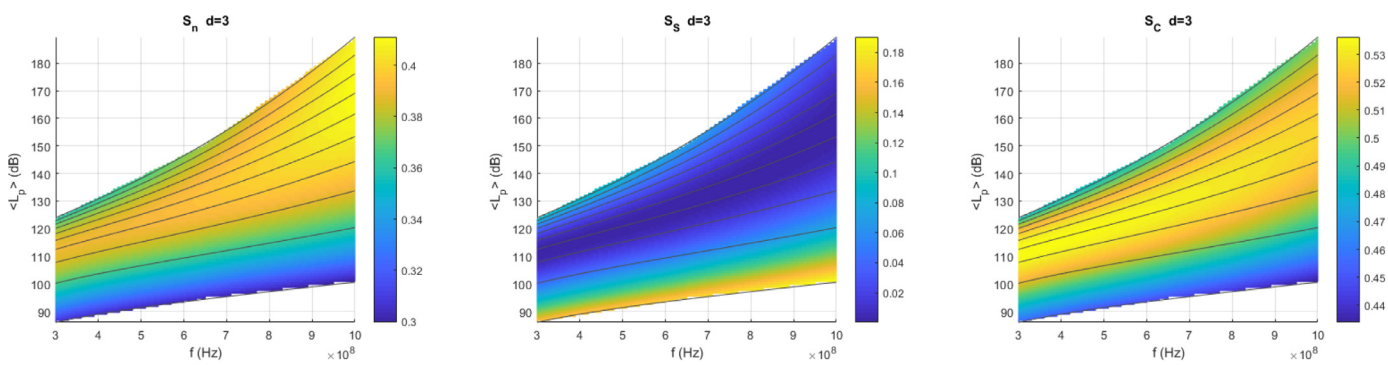

Fig. 3. Single path model: variations of S_n, S_S, S_C in case of loam in the $(\langle L_p \rangle, f)$ plane. Grey lines denote constant values for m_v between 0.05 (the lowest) and 0.5 (the highest), with a constant step of 0.05.

technique (Ghanem and Spanos, 1991; Sudret, 2008; Wiener, 1938). With this method, we approximate the response surface, which is the path loss for diverse values of soil moisture and operating frequency, in the random parameter space given by the joint *pdf* of the uncertain texture parameters.

This paper is arranged as follows. In Section 2, we present the mathematical model and its PCE-based reduction for the purposes of GSA. In Section 3, we provide maps of GSA metrics in the parameter space, with a focus on three soil types, namely clay-loam(CL), loam (L) and sandy-loam (SL), and on an operating frequency of either $f = 0.868$ GHz (LoRa) or $f = 0.433$ GHz (ISM band); a discussion on practical implications of our results is also provided in this Section. Major conclusions drawn from our study are presented in Section 4.

2. Material and methods

2.1. Equations

We start considering a single path model to study EM wave propagation through the soil at high burial depths (typically > 0.5m). In this case, from (2) to (3), it is possible to represent the overall path loss, L_p, in dB as follows (Vuran and Silva, 2009):

$$L_p = L_0 + L_s = 6.4 + 20\log d + 20\log\beta + 8.69\alpha d. \tag{7}$$

Based on (5) and introducing the complex permittivity of the medium $\varepsilon_c = \varepsilon\left[1 - i\left(\frac{\sigma}{\omega\varepsilon}\right)\right] = \varepsilon' - i\varepsilon''$ (both ε' and ε'' are in F/m), constants α and β can be rewritten as

$$\alpha, \beta = \omega\sqrt{\frac{\mu\varepsilon'}{2}\left[\sqrt{1 + \left(\frac{\varepsilon''}{\varepsilon'}\right)^2} \mp 1\right]}. \tag{8}$$

We resort to the semi-empirical model proposed by Peplinski et al. (1995) which provides expressions for ε' and ε'' as

$$\varepsilon' = 1.15\left[1 + \frac{\rho_b}{\rho_s}\left(\varepsilon_s^{\alpha'} - 1\right) + m_v^{\beta'}\left(\varepsilon'_{fw}\right)^{\alpha'} - m_v\right]^{\frac{1}{\alpha'}} - 0.68, \tag{9}$$

$$\varepsilon'' = \left[m_v^{\beta''}\left(\varepsilon''_{fw}\right)^{\alpha'}\right]^{\frac{1}{\alpha'}}, \tag{10}$$

where m_v [−] is the volumetric moisture content, $\rho_s = 2.66\text{g/cm}^3$ is the specific density of solid soil particles, and $\rho_b = \rho_s(1-n)$ is the bulk density, with n [−] the soil porosity; $\alpha' = 0.65$ and $\varepsilon_s = 4.7$ F/m , which is the soil solid permittivity, are empirically determined constants (Dobson et al., 1985), while β' and β'' are empirically determined as functions of soil texture based on mass fractions of sand (S = sand mass / total dry mass) and clay (C = clay mass / total dry mass): $\beta' = 1.2748 - 0.519S - 0.152C$, $\beta'' = 1.33797 - 0.603S - 0.166C$. The quantities ε'_{fw} $[F/m]$ and ε''_{fw} $[F/m]$ are the real and imaginary parts of the relative dielectric constant of free water given by

$$\varepsilon'_{fw} = \varepsilon_{w\infty} + \frac{\varepsilon_{w0} - \varepsilon_{w\infty}}{1 + \left(2\pi f\tau_w\right)^2}, \tag{11}$$

$$\varepsilon''_{fw} = \frac{2\pi f\tau_w\left(\varepsilon_{w0} - \varepsilon_{w\infty}\right)}{1 + \left(2\pi f\tau_w\right)^2} + \frac{\sigma_{eff}\left(\rho_s - \rho_b\right)}{2\pi f\varepsilon_0\rho_s m_v}, \tag{12}$$

where f $[Hz]$ is the frequency, τ_w $[s]$ is the relaxation time for water, $\varepsilon_{w0} = 80.1$ F/m (at20°C) is the static dielectric constant for water, $\varepsilon_{w\infty} = 4.9$ F/m is the high-frequency limit of ε'_{fw}, and ε_0 $[F/m]$ is the permittivity of free space. Peplinski et al. (1995) provide a value of 0.58×10^{-10}s for the product $2\pi\tau_w$ and define, for a range of low frequencies $[0.3 \div 1\text{GHz}]$, an empirical equation to estimate the effective conductivity $[S/m]$: $\sigma_{eff} = 0.0467 + 0.2204\rho_b - 0.4111S + 0.6614$.

In case of devices buried in proximity of the ground surface, we need to consider a two-path model to account for the reflection effect on the

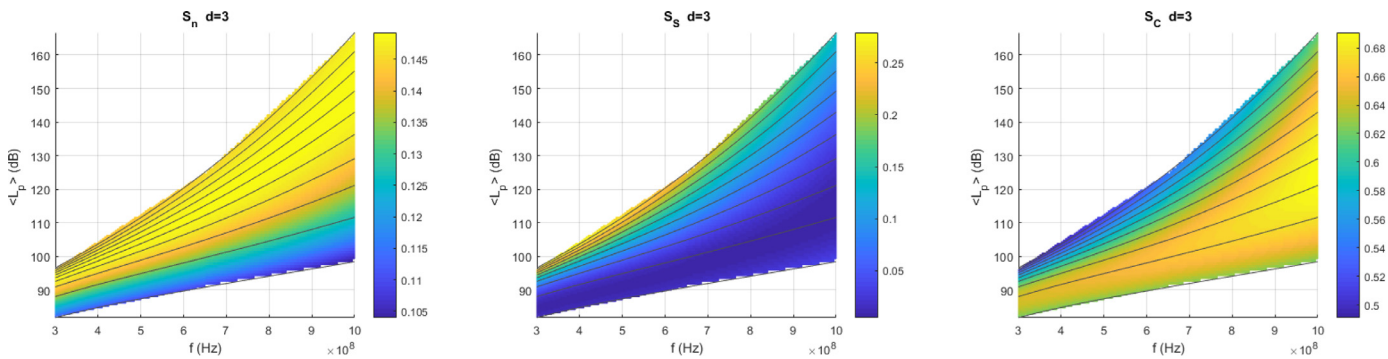

Fig. 4. Single path model: variations of S_n, S_S, S_C in case of sandy-loam in the ($\langle L_p \rangle$, f) plane. Grey lines denote constant values for m_v between 0.05 (the lowest) and 0.5 (the highest), with a constant step of 0.05.

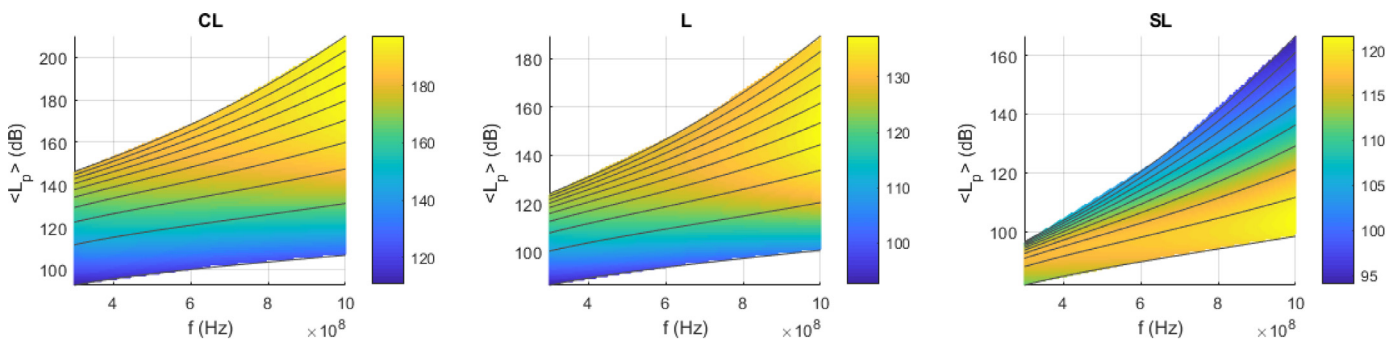

Fig. 5. Single path model: maps of variance in case of clay-loam (CL), loam (L) and sandy-loam (SL) in the ($\langle L_p \rangle$, f) plane. Grey lines denote constant values for m_v between 0.05 (the lowest) and 0.5 (the highest), with a constant step of 0.05.

underground signal propagation (Li et al., 2007). In this case, the total path loss is defined in dB as

$$L_f = L_p - V_{dB}, \tag{13}$$

where $V_{dB} = 10logV^2$ [dB] is the attenuation factor due to the second path, and $V^2 = 1 + \left(\Gamma e^{-\alpha\Delta r}\right)^2 - 2\Gamma e^{-\alpha\Delta r} cos(\pi - \phi + 2\pi/\lambda\Delta r)$; $\Delta r = r - d$ [m] is the difference between the two paths, Γ and ϕ the amplitude and phase angle of the reflection coefficients at the reflection point (Vuran and Silva, 2009).

2.2. Global sensitivity analysis

Most sensitivity analyses in literature are still local or one parameter at a time, thus relying on the assumptions of model linearity and additivity (Ferretti et al., 2016). Here, we employ a global approach to perform sensitivity analysis in order to overcome these limits and explore simultaneously the full range of variation of key texture parameters. In this way, it is possible to: (i) handle interaction effects among input uncertainties and (ii) clearly identify how uncertainty in the output of a model can be apportioned to different sources of uncertainty in input. Among global approaches, we resort to widely used variance-based metrics, the Sobol' indices, which pinpoints for which sources of uncertainty additional data should be collected to narrow the variance associated with model predictions (Saltelli et al., 2000; Sobol', 1993).

Variabilities of porosity (n), and sand and clay contents (S, C) reflect the uncertainty in soil texture. For the sake of simplicity and consistency with the model presented in Section 2.1, we adopt a zonation approach (Ciriello et al., 2017) and we assume that the soil consists of a single uniform stratum of either clay-loam (CL), loam (L) or sandy-loam (SL). We assign to each type of soil the mean and standard deviation identified by Carsel and Parrish (1988) as presented in Table 1. We apply GSA to identify, for each soil, the regions of influence of soil texture parameters in the (m_v, f, d) space. To do this, we derived a truncated polynomial

Table 1
Statistical distributions (PDFs) and properties (mean, $\langle \cdot \rangle$, and standard deviation, σ) of the uncertain model parameters.

Parameter	PDF	Clay-loam	Loam	Sandy-loam
n	Normal	$\langle n \rangle = 0.41$	$\langle n \rangle = 0.43$	$\langle n \rangle = 0.41$
		$\sigma_n = 0.09$	$\sigma_n = 0.10$	$\sigma_n = 0.09$
S	Lognormal	$\langle S \rangle = 29.8$	$\langle S \rangle = 40$	$\langle S \rangle = 63.4$
		$\sigma_S = 5.9$	$\sigma_S = 6.5$	$\sigma_S = 7.9$
C	Lognormal	$\langle C \rangle = 32.6$	$\langle C \rangle = 19.7$	$\langle C \rangle = 11.1$
		$\sigma_C = 3.7$	$\sigma_C = 5.2$	$\sigma_C = 4.8$

chaos expansions (PCE) (Wiener, 1938) which approximates L_p as

$$L_p(m_v, f, d; \mathbf{P}) \approx \sum_{j=0}^{N_Q-1} a_j(m_v, f, d)\Psi_j(\mathbf{P}), \quad N_Q = \frac{(N_{\text{par}} + N_{\text{pol}})!}{N_{\text{par}}!N_{\text{pol}}!}, \tag{14}$$

where $\mathbf{P} = \{n, S, C\}$ is the vector of uncertain texture parameters, and $\Psi_j(\mathbf{P})$ denotes multivariate Hermite polynomials. We use the Stochastic Collocation (SC) method (Webster et al., 1996) to compute the deterministic expansion coefficients a_j. The zero-order coefficient, $a_0(m_v, f, d)$, corresponds to the mean of L_p, i.e., $\langle L_p(m_v, f, d) \rangle = a_0(m_v, f, d)$. The variance of L_p is computed as

$$\sigma^2_{L_p}(m_v, f, d) = \sum_{j=1}^{N_Q-1} a_j^2(m_v, f, d)\langle \Psi_j^2(\mathbf{P}) \rangle, \tag{15}$$

which is derived from (14) by accounting for the orthogonality of the Hermite polynomials, $\langle \Psi_i \Psi_k \rangle = 0$ for all $i \neq k$.

The SC is well suited for the low-dimensional probability spaces, such as $N_{\text{par}} = 3$ considered in the present study (e.g., Ciriello et al., 2013a; 2015; 2013b, and the references therein).

The Sobol' indices (Sobol', 1993) provide a metric of the relative impact of each parameter affected by uncertainty (see Table 1) on the overall predictive uncertainty, as quantified by (15). The contribution of the

ith parameter, P_i to the response variance is quantified by a "principle sensitivity index" $\mathcal{S}_i$, which is defined, based on the PCE approximation, by (Sudret, 2008)

$$\mathcal{S}_i(m_v, f, d) = \frac{\sigma^2_{L_p,i}}{\sigma^2_{L_p}}, \qquad \sigma^2_{L_p,i}(m_v, f, d) = \sum_{\gamma\in\Gamma_i} a^2_\gamma(m_v, f, d)\langle\Psi^2_\gamma(P_i)\rangle, \tag{16}$$

where $\Gamma_i = \{\gamma \in (1, \ldots, N_Q - 1) : \Psi_\gamma(P_i)\}$. This definition can be easily extended to evaluate the joined influence of a subset of model parameters, in case that principle sensitivity indices do not provide a full description of the response variance. The Sobol indices computed for all the possible subsets of parameters sum up to unity (Sobol', 1993).

Global sensitivity metrics, including the Sobol' indices, are generally computed by means of Monte Carlo simulations (Sobol', 2001). However, depending on the complexity of model equations and the number of uncertain parameters, the deriving computational cost may discourage the use of global approaches for sensitivity analysis. In these cases, metamodeling techniques (among which PCE is one option) represent powerful tools to accelerate the computational cost associated with GSA and other onerous stochastic analyses. For the purposes of this study, the approximation of the response surface with PCE is build upon soil texture uncertainty, while leaving information on the variability of operating conditions (d and f) within the deterministic coefficients a_j. This is done to distinguish among epistemic uncertainty and response variability due to the design/operating parameters.

3. Results and discussion

Here, we provide results of GSA for the single path transmission mechanism based on a second-order PCE, which provides an accurate approximation of the model response surface (not shown) and requires only 10 full model runs to be calibrated.

GSA results are presented in Figs. 2–4 for clay-loam, loam and sandy-loam, respectively. These Figures depict $\langle L_p\rangle$ vs f, in the range 0.3–1 GHz, for constant values of m_v between 0.05 and 0.5. Within the area delimited by the curves correspondent to $m_v = 0.05$ and $m_v = 0.5$, we explore variation of sensitivity indices. For the sake of brevity, for each selected soil type, we represent the case of two devices at a distance $d = 3$ m. This is a reasonable configuration for practical applications. Nevertheless, we also performed GSA in case of d=1–6 m (not shown) and we observed that the Sobol indices are not significantly affected by this parameter.

In case of clay-loam, the principal sensitivity indices associated with n, S and C are depicted in Fig. 2. It is shown that, generally, the indices exhibit a negligible variation with f, while it is relevant to analyze their behavior with respect to m_v. Influence of n, as denoted by S_n values, is always above 0.6 and increases with m_v till about 0.85 when the water content tends to 0.5. Regarding to at the principal sensitivity index associated with S, an opposite behavior, respect to m_v variations, is detected. Specifically, the sand content is relevant ($S_S > 0.1$) in case of low values of m_v, (< 0.15), with a maximum of about 0.25 for $m_v = 0.05$. The principal sensitivity index of C exhibits a very low variation with m_v within the range 0.14–0.17. Maximum values for S_C are reached in a middle range of water content values between 0.1 and 0.3.

In case of loam, the principal sensitivity indices associated with n, S and C are depicted in Fig. 3. Also in this case the indices exhibit a low variation with f. Regarding to S_n, it varies within the range 0.3–0.4, and is maximum for high values of both m_v and f. When looking at S_S, it is possible to observe that the sand content is relevant ($S_S > 0.1$) in case of low values of m_v, (< 0.1), with a maximum of about 0.2 for $m_v = 0.05$. The principal sensitivity index of C exhibits a low variation with m_v within the range 0.44–0.53. Maximum values for S_C are reached in a middle range of water content values between 0.1 and 0.3.

In case of sandy-loam, the principal sensitivity indices associated with n, S and C are depicted in Fig. 4. Regarding to S_n, its value is almost constant with respect to f and increases weakly with m_v within the range 0.1–0.15. When looking at S_S, it is possible to observe a moderate decrease when f increases and that the sand content is relevant ($S_S > 0.1$) in case of high values of m_v, (> 0.25), with a maximum of about 0.3 when m_v tends to 0.5. The principal sensitivity index of C increases with f and exhibits a moderate variation with m_v within the range 0.5–0.68. Maximum values for S_C are reached in the range of water content values 0.1–0.3.

Table 2
Single path model: GSA outcomes for two possible experimental settings with $d = 3$m and $f = 0.868$ GHz or $f = 0.433$ GHz.

f	Soil type	$\langle L_p\rangle$ (dB)	m_v range	influential parameters
0.868 GHz	CL	105–151	0.05–0.19	S_n =0.58–0.79 S_S =0.26–0.03 S_C =0.14–0.16
0.868 GHz	L	98–151	0.05–0.30	S_n = 0.30–0.40 S_S =0.18–0.00 S_C =0.44–0.53
0.868 GHz	SL	96–150	0.05–0.50	S_n = 0.11–0.15 S_S =0.03–0.18 S_C =0.63–0.58
0.433 GHz	CL	97–151	0.05–0.40	S_n =0.59–0.82 S_S =0.25–0.01 S_C =0.15–0.16
0.433 GHz	L	90–133	0.05–0.50	S_n =0.31–0.36 S_S =0.16–0.09 S_C =0.45–0.48
0.433 GHz	SL	86–106	0.05–0.50	S_n =0.11–0.14 S_S =0.01–0.27 S_C =0.62–0.50

Table 2 focuses on GSA results for two experimental settings in which the two devices, at a distance $d = 3$ m, work with an operating frequency of either $f = 0.868$ GHz (LoRa) or $f = 0.433$ GHz (ISM band), and are able to detect path losses $L_p \leq 151$ dB. Under these conditions, the range of measurable path loss increases with the grain size of the soil, as already shown in Figs. 2–4. As a consequence, for $f = 0.868$ GHz, in case of clay-loam it is possible to have only an estimate of m_v if ≤ 0.19; while for loam and sandy-loam, it is possible to estimate m_v if ≤ 0.30 and ≤ 0.50, respectively. For the selected frequency and within the detectable range of L_p values, we observe that for the clay-loam the variability of n is responsible for the 58–79% of the uncertainty related to the estimate; hence, this parameter has to be estimated with high accuracy in order to reduce the predictive uncertainty. While influence of C is almost constant and responsible in average for only the 15% of the predictive uncertainty, influence of S varies significantly and only for the minimum detectable values of L_p it is quite significant contributing for a maximum of 26% to the predictive uncertainty. For a loamy soil, n and C are both important with an average contribution of about 35% and 49%, respectively. Again, the influence of S is associated with the highest variability with a maximum contribution of 18% for the minimum detectable L_p. Finally, in case of sandy-loam, the most important parameter is C which is responsible in average for the 60% of the predictive uncertainty; influence of n is low (about 13%) and almost constant, while the contribution of S shows again a variability and in this case it has a maximum of 18% for the maximum measurable value of L_p.

When considering $f = 0.433$ GHz, in case of clay-loam it is possible to have an estimate of m_v if ≤ 0.40; while for loam and sandy-loam, it is possible to estimate m_v if ≤ 0.50. It is shown that the results do not exhibit significant differences with respect to the other operating frequency. This is in line with the general observation that sensitivity indices vary more with m_v than with f. The main difference exists in the range of values of m_v that can be estimated; this range is wider since L_p decreases with f.

The sensitivity metrics discussed above, show how the predictive uncertainty can be apportioned to the different sources of uncertainty in the model input. In order to quantify the predictive uncertainty for the three selected soil types, Fig. 5 represents the map of variance

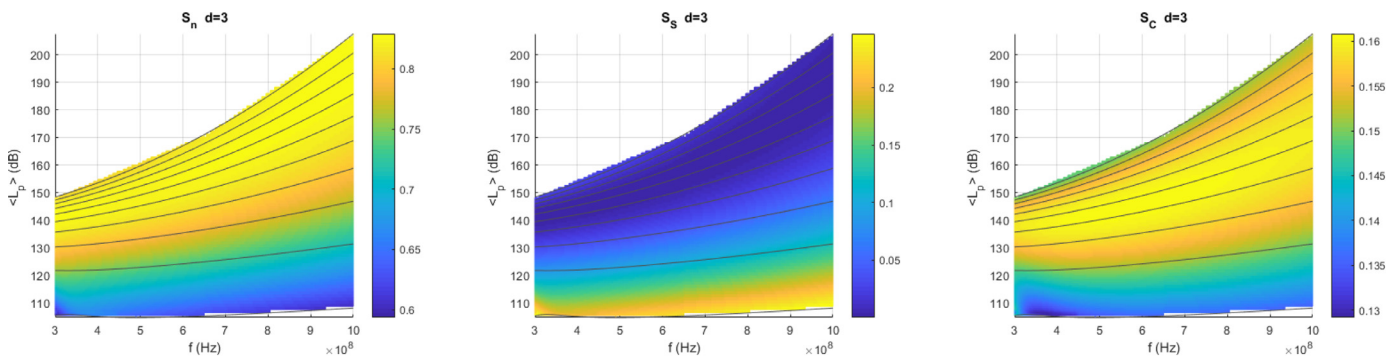

Fig. A1. Two-path model: variations of S_n, S_S, S_C in case of clay-loam in the $(\langle L_p \rangle, f)$ plane. Grey lines denote constant values for m_v between 0.05 (the lowest) and 0.5 (the highest), with a constant step of 0.05.

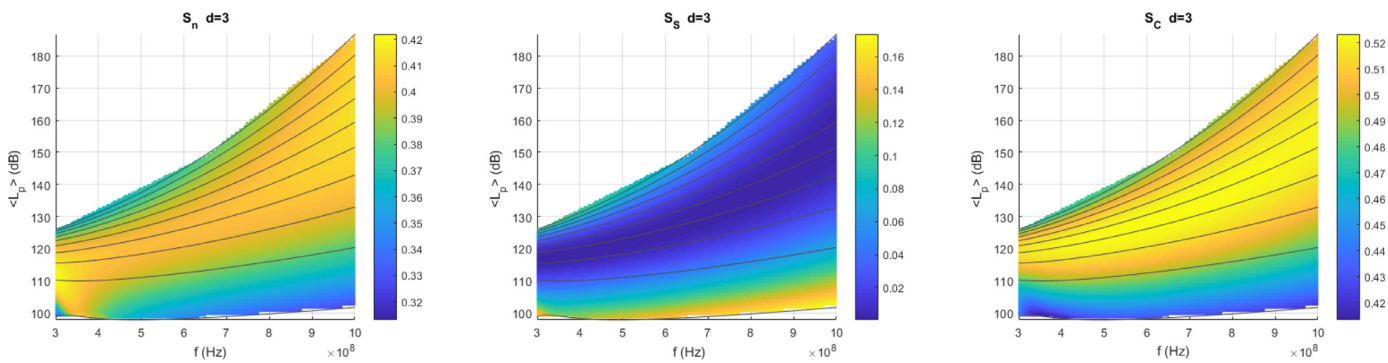

Fig. A2. Two-path model: variations of S_n, S_S, S_C in case of loam in the $(\langle L_p \rangle, f)$ plane. Grey lines denote constant values for m_v between 0.05 (the lowest) and 0.5 (the highest), with a constant step of 0.05.

associated with L_p in the selected (m_v, f) domain and for $d = 3$m (it is not shown but the variance always increases with d). As expected, $\sigma^2_{L_p}$ increases with f. In case of clay-loam and loam, $\sigma^2_{L_p}$ also increases with m_v; the opposite is detected for sandy-loam. We also note that the variance decreases when the grain size increases.

In field scale applications, when L_p is available from device's reading, it is possible to use Figs. 2–4 to determine m_v and identify which texture parameters have to be more accurately estimated to reduce the predictive uncertainty. In this sense, results of GSA can be read with respect to soil moisture, given the correspondence between m_v and L_p when texture and operating parameters are fixed. Note that results of GSA with respect to L_p, i.e. the device's reading, may represent a basis for the application of other techniques, such as data assimilation, sensitivity-based model calibration, or model selection (Ciriello et al., 2015; 2013b), in order to reduce the epistemic uncertainty and increase the reliability of m_v estimations at the same time.

In case of a two-path transmission mechanism, results of GSA are very similar as shown in Appendix A.

4. Conclusions

In this work we characterize the predictive uncertainty associated with the path loss when adopting WUCNs to estimate soil moisture. In particular, we focus on uncertainty deriving from textural parameters which significantly influence the path loss of the signal transmitted to the receiver as expressed in the selected underlying mathematical framework. We perform GSA and propagate texture uncertainty based on the PCE technique to reduce the computational cost associated with the analysis. We produce sensitivity and variance maps in order to fully characterize the predictive uncertainty as a guide for practical applications and we apply our methods to: (i) different transmission mechanisms (either single path or two-path models), (ii) different device distances (1–6 m), and (iii) three soil types (clay-loam, loam, and sandy-loam).

Our study reveals that $\langle L_p \rangle$ varies significantly with the operating parameters, f and d, for given soil texture and moisture, and the same is true for the predictive uncertainty (i.e. $\sigma^2_{L_p}$). At the same time, the operating conditions have a negligible impact on the selected sensitivity indices. This means that the most influential texture parameters, which may deserve additional data collection, vary only with soil type and moisture. This is relevant in field scale applications, where d and f are typically controlled by spatial and/or technological constraints.

We also find that the transmission mechanism (see Appendix A) does not impact significantly on GSA results and on the predictive uncertainty.

GSA reveals that if in case of clay-loam, variability on the porosity explains most of the predictive uncertainty, in case of sandy-loam the clay content is the parameter which requires the most accurate estimate. When considering a loamy soil, these two parameters are almost equally important. Influence of sand content is significantly variable for the three soil types: it increases with m_v in case of sandy-loam, while the opposite happens when considering the other two soils. In general, sensitivity indices exhibit significant variations with m_v.

Our findings can be easily extended to other soil types. At the same time, in a future analysis, we want to extend our approach in order to consider alternative models, respect to the one suggested by Peplinski et al. (1995), and evaluate their predictive capacity against measurements, following the method suggested in Ciriello et al. (2015, 2013b).

Acknowledgments

This work was supported in part by the European Project BRIGAID (Project ID: 700699). There are no data sharing issues since all of the

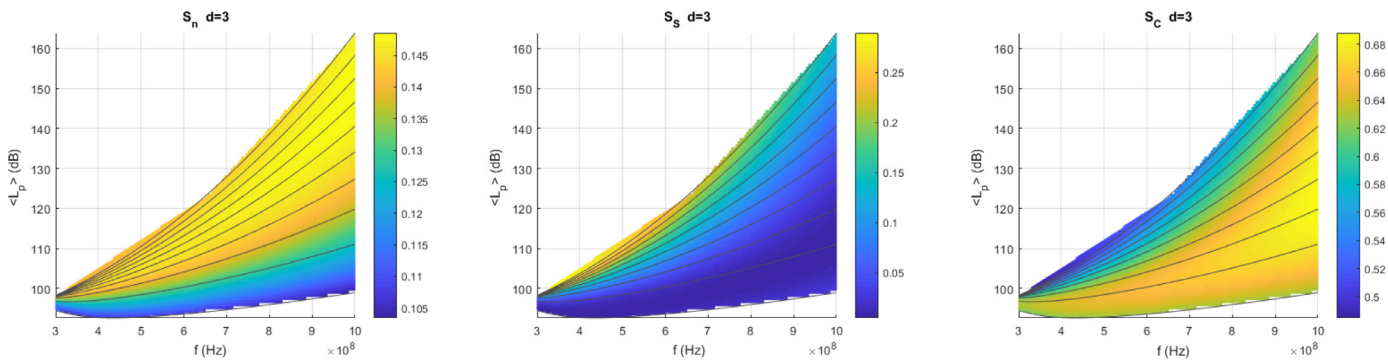

Fig. A3. Two-path model: variations of S_n, S_S, S_C in case of sandy-loam in the $(\langle L_p \rangle, f)$ plane. Grey lines denote constant values for m_v between 0.05 (the lowest) and 0.5 (the highest), with a constant step of 0.05.

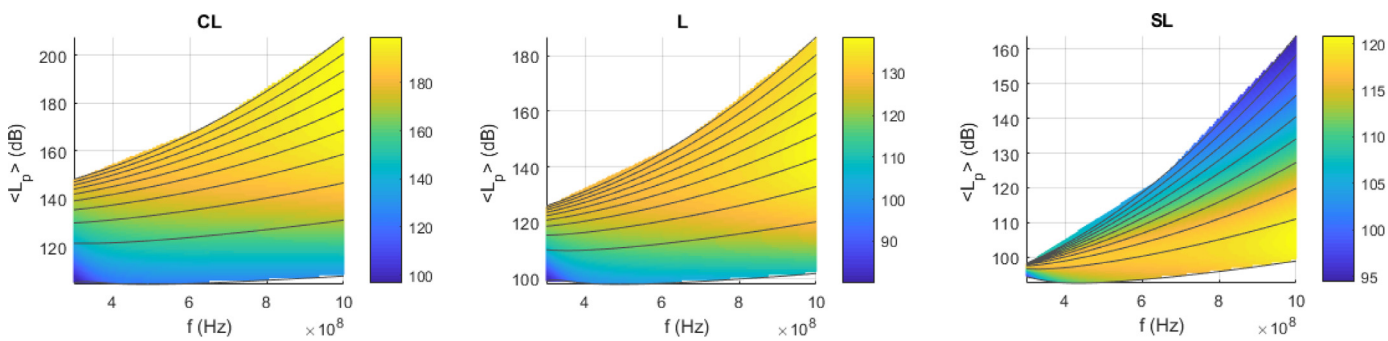

Fig. A4. Two-path model: maps of variance in case of clay-loam (CL), loam (L) and sandy-loam (SL) in the $(\langle L_p \rangle, f)$ plane. Grey lines denote constant values for m_v between 0.05 (the lowest) and 0.5 (the highest), with a constant step of 0.05.

Table A1
Two-path model: GSA outcomes for two possible experimental settings with $d = 3$m and $f = 0.868$ GHz or $f = 0.433$ GHz.

f	Soil type	$\langle L_p \rangle$ (dB)	m_v range	influential parameters
0.868 GHz	CL	107–151	0.05–0.19	S_n =0.61–0.80
				S_S =0.24–0.03
				S_C =0.14–0.16
0.868 GHz	L	100–151	0.05–0.31	S_n =0.33–0.41
				S_S =0.17–0.01
				S_C =0.43–0.52
0.868 GHz	SL	96–143	0.05–0.50	S_n =0.11–0.15
				S_S =0.02–0.19
				S_C =0.63–0.57
0.433 GHz	CL	105–151	0.05–0.39	S_n =0.65–0.82
				S_S =0.21–0.01
				S_C =0.13–0.16
0.433 GHz	L	98–133	0.05–0.50	S_n =0.37–0.37
				S_S =0.13–0.10
				S_C =0.42–0.48
0.433 GHz	SL	93–106	0.05–0.50	S_n =0.11–0.14
				S_S =0.01–0.27
				S_C =0.62–0.50

numerical information is provided in the figures produced by solving the equations in the paper.

Appendix A. Influence of two-path transmission

Results presented below refer to a couple of devices at a distance $d = 3$ m and depth $z_1 = z_2 = 0.2$ m. In this configuration, the ground surface is responsible for reflection of the signal towards the receiver.

Figs. A.6–A.8 depict the same results of Figs. 2–4, for the two-path transmission mechanism. The same holds for Table A.3 and Fig. A.9 with respect to Table 2 and Fig. 5. It is possible to observe that GSA results, as well as the variance of the response, are very similar to those derived for the single path model. Main differences involve the trend of $\langle L_p \rangle(f)$ curves for constant m_v, especially for low path loss values. Given these results, and considering that in the most of applications the single path mechanism holds, it seems not relevant to analyze the effect of ground surface reflection if the aim is to understand which parameter influences more the predictive uncertainty. Furthermore, the two-path model includes a couple of additional parameters, ϕ and Γ, thus making calibration challenging in practical applications. As such, it seems generally convenient to perform GSA and uncertainty quantification on the single path model, in order to characterize and reduce the predictive uncertainty, by addressing measurements towards the most significant parameters.

References

Ahmad, M., Chakraborty, D., Aggarwal, P., Bhattacharyya, R., Singh, R., 2018. Modelling soil water dynamics and crop water use in a soybean-wheat rotation under chisel tillage in a sandy clay loam soil. Geoderma 327, 13–24. Cited By 0

Akyildiz, I.F., Stuntebeck, E.P., 2006. Wireless underground sensor networks: research challenges. Ad Hoc Netw. 4 (6), 669–686.

Akyildiz, I.F., Sun, Z., Vuran, M.C., 2009. Signal propagation techniques for wireless underground communication networks. Phys. Commun. 2 (3), 167–183.

Assouline, S., Ciriello, V., Tartakovsky, D.M., 2017. Estimation of intrinsic length scales of flow in unsaturated porous media. Water Resour. Res. 53 (11), 9980–9987.

Balanis, C.A., 2012. Advanced Engineering Electromagnetics. Wiley.

Bittelli, M., 2011. Measuring soil water content: a review. HortTechnology 21 (3), 293–300.

Brandhorst, N., Erdal, D., Neuweiler, I., 2017. Soil moisture prediction with the ensemble kalman filter: handling uncertainty of soil hydraulic parameters. Adv. Water. Resour. 110, 360–370.

Carsel, R.F., Parrish, R.S., 1988. Developing joint probability distributions of soil water retention characteristics. Water Resour. Res. 24(5), 755–769.

Ciriello, V., Di Federico, V., Riva, M., Cadini, F., De Sanctis, J., Zio, E., Guadagnini, A., 2013. Polynomial chaos expansion for global sensitivity analysis applied to a model of radionuclide migration in a randomly heterogeneous aquifer. Stoch. Environ. Res. Risk Assess. 27, 945–954.

Ciriello, V., Edery, Y., Guadagnini, A., Berkowitz, B., 2015. Multimodel framework for characterization of transport in porous media. Water Resour. Res. 51(5), 3384–3402.

Ciriello, V., Guadagnini, A., Di Federico, V., Edery, Y., Berkowitz, B., 2013. Comparative analysis of formulations for conservative transport in porous media through sensitivity-based parameter calibration. Water Resour. Res. 49 (9), 5206–5220.
Ciriello, V., Lauriola, I., Bonvicini, S., Cozzani, V., Di Federico, V., Tartakovsky, D.M., 2017. Impact of hydrogeological uncertainty on estimation of environmental risks posed by hydrocarbon transportation networks. Water Resour. Res. 53, WR021368.
Dobriyal, P., Qureshi, A., Badola, R., Hussain, S.A., 2012. A review of the methods available for estimating soil moisture and its implications for water resource management. J. Hydrol. 458–459, 110–117.
Dobson, M.C., Ulaby, F.T., Hallikainen, M.T., El-Rayes, M.A., 1985. Microwave dielectric behavior of wet soil - part ii: dielectric mixing models. IEEE Trans. Geosci. Remote Sens. 33(3), 803–807.
Dong, X., Vuran, M.C., Irmak, S., 2013. Autonomous precision agriculture through integration of wireless underground sensor networks with center pivot irrigation systems. Ad Hoc Netw. 11 (7), 1975–1987.
Ferretti, F., Saltelli, A., Tarantola, S., 2016. Trends in sensitivity analysis practice in the last decade. Sci. Total Environ. 568, 666–670.
Ghanem, R.G., Spanos, P.D., 1991. Stochastic Finite Elements-ASpectral Approach. Springer, Berlin.
Huang, J., McBratney, A.B., Minasny, B., Triantafilis, J., 2017. Monitoring and modelling soil water dynamics using electromagnetic conductivity imaging and the ensemble kalman filter. Geoderma 285, 76–93.
Li, L., Vuran, M. C., Akyildiz, I. F., 2007. Characteristics of underground channel for wireless underground sensor networks. Vol. Med-Hoc-Net 07, Corfu, Greece., p. 95.
Martnez-Fernndez, J., Gonzlez-Zamora, A., Snchez, N., Gumuzzio, A., 2015. A soil water based index as a suitable agricultural drought indicator. J. Hydrol. 522, 265–273.
Moghadas, D., Jadoon, K.Z., McCabe, M.F., 2017. Spatiotemporal monitoring of soil water content profiles in an irrigated field using probabilistic inversion of time-lapse emi data. Adv. Water Resour. 110, 238–248.
Narasimhan, B., Srinivasan, R., 2005. Development and evaluation of soil moisture deficit index (smdi) and evapotranspiration deficit index (etdi) for agricultural drought monitoring. Agric. For. Meteorol. 133 (1), 69–88.
Peplinski, N.R., Ulaby, F.T., Dobson, M.C., 1995. Dielectric properties of soils in the 0.31.3-ghz range. IEEE Trans. Geosci. Remote Sens. 33(3), 803–807.
Saltelli, A., Chan, K., Scott, E.M., 2000. Sensitivity Analysis. Wiley.
Sheffield, J., Wood, E.F., 2008. Global trends and variability in soil moisture and drought characteristics, 19502000, from observation-driven simulations of the terrestrial hydrologic cycle. J. Clim. 21 (3), 432–458.
Sobol', I.M., 1993. Sensitivity estimates for nonlinear mathematical models. Math. Model. Comput. 1, 407–414.
Sobol', I.M., 2001. Global sensitivity indices for nonlinear mathematical models and their Monte Carlo estimates. Math. Comput. Simul. 55, 271–280.
Sudret, B., 2008. Global sensitivity analysis using polynomial chaos expansions. Reliab. Eng. Syst. Saf. 93, 964–979.
Tartakovsky, D.M., 2013. Assessment and management of risk in subsurface hydrology: a review and perspective. Adv. Water Resour. 51, 247–260.
Vuran, M.C., Silva, A.R., 2009. Communication through soil in wireless underground sensor networkstheory and practice. Sens. Netw. 309–318.
Webster, M., Tatang, M.A., McRae, G.J., 1996. Application of the probabilistic collocation method for an uncertainty analysis of a simple ocean model. Technical Report, MIT joint program on the science and policy of global change reports series No. 4. MIT, Cambridge, MA.
Wiener, N., 1938. The homogeneous chaos. Am. J. Math. 60, 897–936.